

Volume-shear coupling in a mesoscopic model of amorphous materials

E. A. Jagla

Centro Atómico Bariloche, Instituto Balseiro, Comisión Nacional de Energía Atómica, CNEA, CONICET, UNCuyo, Av. E. Bustillo 9500 (R8402AGP) San Carlos de Bariloche, Río Negro, Argentina

We present a two-dimensional mesoscopic model of a yield stress material that includes the possibility of local volume fluctuations, in such a way that the shear strength of the material decreases as the local density decreases. The model reproduces a number of effects well known in the phenomenology of this kind of materials. Particularly, we find that: the volume of the sample increases as the deformation rate increases; shear bands are no longer oriented at 45° with respect to the principal axis of the applied stress (as in the absence of volume fluctuations); homogeneous deformation becomes unstable at low enough deformation rates if volume-shear coupling is strong enough. We also analyze the implications of this coupling in the context of out of equilibrium shear bands appearing for instance in metallic glasses.

I. INTRODUCTION

Dilatancy [1, 2] is a general property of granular and other kind of amorphous materials. It is characterized by a volume increase observed when the material is forced to shear. Traditionally, dilatancy has been known to play an important role in the mechanics of soils and sands [3–6]. However, dilatancy may be considered as a particular case of volume-shear coupling phenomena, that are also relevant for instance in the physics of shear stress fluids (most of which in fact have some kind of “grains” as elementary constituents). [7–11] Also a volume change, and therefore a volume-shear coupling has been invoked as one important ingredient of the physics of materials failing by the nucleation of shear bands, particularly metallic glasses. [12–15]

We investigate here the dilatancy effect and the volume-shear coupling in a mesoscopic model of the yielding transition. Previously [16–18], this model has been applied to situations where the local density of the system was not considered to play an important role, and actually the possible change of density was not even considered. Here, we study the coupled evolution of local strain and local density, and address the influence of local density fluctuations in the shearing behavior of the system.

The paper is organized as follows. In the next section we consider a prototypical one variable, mean field model of the yielding behavior and add to it an additional variable describing density changes. We obtain in this simple model the basic properties of the dilatancy effect, particularly, the increase in system volume with the increase of strain rate in the system. Then in Section III we show how this behavior justifies that in spatially extended models the geometric orientation of plastically deformed regions, or shear bands, is rotated with respect to the case in which there is no such volumetric effect. The orientation we observe can be qualitatively explained with the classical Mohr-Coulomb failure criterion. In section IV we show that volume-shear coupling can produce a flowing state in the material in which parts of the sample yield and have a lower density, while other

parts remain essentially rigid, and with a higher density. While all previously mentioned results correspond to equilibrium and reversible situations, in Section V we investigate the important case in applications of samples prepared by some sort of annealing, which are then submitted to a shear deformation until they fail, typically by nucleating a non-equilibrium shear band, as it occurs in metallic glasses. Finally, in Section VI, we summarize and conclude.

II. COUPLING VOLUME AND SHEAR IN A ONE-SITE MODEL

We start by considering a very simple model with two degrees of freedom (representing the shear and volume state of a sample) and study the appearance of a dilatancy effect. We take as a starting point the well known Prandtl-Tomlinson model of friction for the shear degree of freedom e_2 [19]. The model is written as a dynamical evolution equation of the form

$$\dot{e}_2 = -\frac{dV(e_2)}{de_2} + (\dot{\gamma}t - e_2)k \quad (1)$$

and it describes the situation depicted in Fig. 1. The driving $\dot{\gamma}t$ pulls from the variable e_2 through a spring of stiffness k . e_2 is also affected by the force $f_2(e_2) \equiv -dV/de_2$. In a friction context f_2 represents the corrugated potential between two surfaces sliding against each other. In a context of yielding, f_2 represents the internal stresses that a small portion of the system feels due to its amorphous nature. In any case, the $f_2(e_2)$ function is expected to have many minima. To fix ideas we will assume here that f_2 is a periodic function. In the traditional form of the PT model the “friction force” is calculated as the average force that the driving has to apply in order to maintain a uniform driving velocity of $\dot{\gamma}$. This force is the one that stretches the spring, so the friction force σ is calculated as

$$\sigma = \langle \dot{\gamma}t - e_2 \rangle k \quad (2)$$

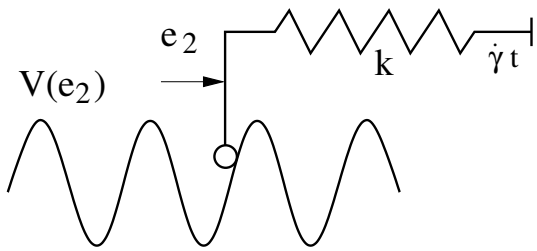


FIG. 1: Schematic representation of the Prandtl-Tomlinson model, mathematically described by Eq. (1).

where the brackets notate a temporal average. In the yielding context, an equation like Eq. (1) is taken as a mean field description of a spatially extended system. In the extended case, $\dot{\gamma}t$ represents the spatial (instantaneous) average of the value of e_2 , namely

$$\dot{\gamma}t = \overline{e_2} \quad (3)$$

and the model equation must be written with the explicit inclusion of the externally applied stress σ in the form

$$\dot{e}_2 = f_2(e_2) + (\overline{e_2} - e_2)k + \sigma \quad (4)$$

In any case, the difference between using Eqs. (1) and (2), or (3) and (4) is irrelevant as the difference amounts to a shift in the instantaneous value of e_2 by a constant, that does not alter the main feature of the flow curve (i.e., the $\dot{\gamma}$ vs σ dependence) of the model.

We will extend now the PT model to include the possibility of volume fluctuations, described by a variable e_1 . The value of e_1 will tend to evolve to its equilibrium value, with a dynamics mainly controlled by the value of the bulk modulus B in the system. Considering an overdamped dynamics, this evolution must be of the form

$$\dot{e}_1 = -Be_1 \quad (5)$$

where the value $e_1 = 0$ was chosen as the equilibrium value in the system. Of course in this trivial form the evolution of e_1 is totally decoupled from the evolution of e_2 , and there is no effect of e_1 (that adjusts at $e_1 = 0$ for all values of $\dot{\gamma}$) on e_2 .

Now we introduce a coupling between e_1 and e_2 that describes a possible dilatancy effect in the system. We expect that if e_1 increases, then the system yields more easily, therefore e_1 must have an effect on the force f_2 . So we do the following. We consider a two dimensional potential energy $V(e_1, e_2)$ from which forces $f_{1,2}$ are obtained as the partial derivatives $f_{1,2} = -\partial V/\partial e_{1,2}$. Therefore, the model equations will be

$$\begin{aligned} \dot{e}_1 &= -\partial V/\partial e_1 \\ \dot{e}_2 &= -\partial V/\partial e_2 + k(\dot{\gamma}t - e_2) \end{aligned} \quad (6)$$

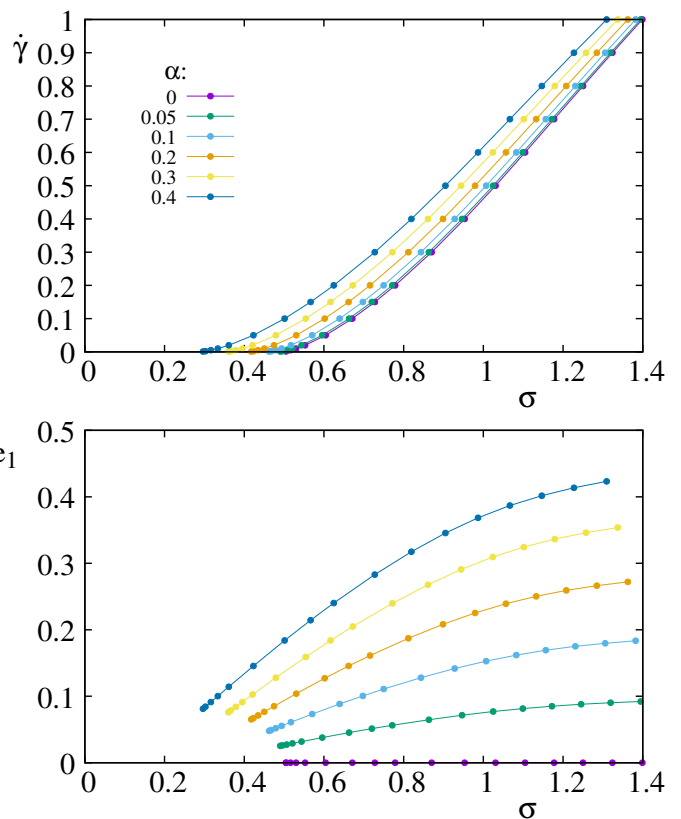


FIG. 2: (a) Flow curves of the one-particle model with coupling between shear and volume degrees of freedom. Different curves correspond to different values of α (Eq. 8) as indicated. (b) Corresponding curves of the temporal average of the variable e_1 representing the increase in system volume, caused by shear. The volume is larger for larger values of α , and also increases with the value of strain rate $\dot{\gamma}$.

The form of $V(e_1, e_2)$ will dictate the form of the effective coupling between the modes e_1 and e_2 . We will use for V the generic form

$$V(e_1, e_2) = \frac{B}{2}e_1^2 + V_1(e_1)V_2(e_2) \quad (7)$$

Note first of all that we isolated the term $Be_1^2/2$ that corresponds to a sample with bulk modulus B . In the second term, $V_2(e_2)$ will be an oscillatory potential with many minima along the e_2 axis. In the case in which the factor $V_1(e_1)$ is a constant, this potential will provide the decoupled model in which e_1 and e_2 evolve separately. However, if the value of $V_1(e_1)$ decreases as e_1 increases a dilatancy effect will be obtained. To lowest order we may consider that the change of V_1 is linear with e_1 . We can conveniently model it as

$$V(e_1, e_2) = \frac{B}{2}e_1^2 + [1 + \tanh(\alpha e_1)]U_2(e_2) \quad (8)$$

This form provides a corrugated potential on e_2 with an

amplitude that tends to 0 when e_1 is positive and large, whereas saturating to an e_1 -independent values for large negative e_1 . Therefore α quantifies the coupling between e_1 and e_2 . Coupling vanishes when $\alpha = 0$.

In the next Section dealing with an extended system we will consider some stochastic form of the function V_2 . Here, it suffices to consider a single periodic expression. In the past we have considered two particular forms of the V_2 term, described as the “cuspy” and “smooth” potential forms, defined as

$$U_2(x) = (x - [x])^2/2 \quad (\text{cuspy}) \quad (9)$$

$$U_2(x) = \sin(x) \quad (\text{smooth}) \quad (10)$$

(the square brackets in the first expression indicates the integer part function). It is seen that the cuspy case consists of a concatenation of parabolic pieces.

Driving along the e_2 direction will produce the effect of modifying the value of e_1 . We simulated Eqs. (6), using expressions (8), (10) for the potential (for concreteness we work out the smooth potential case), at different levels of the coupling α . The flow curve $\dot{\gamma}$ as a function of σ and the temporarily averaged values of e_1 are reported in Fig. 2. We see how the volume e_1 increases as $\dot{\gamma}$ (or σ) increases. This is the dilatancy effect. The effect is stronger as the value of α increases. Note also how the flow curve for larger values of α shifts to the left (and in particular the critical stress reduces) at larger α when e_1 is positive.

The dilatancy effect in the PT model is the germ of a couple of interesting features that we will encounter in the spatially extended model, and that are analyzed in the next two sections.

III. FLOW CURVES AND ORIENTATION OF SHEAR BANDS IN THE PRESENCE OF DILATANCY

In a spatially extended system, and in the absence of volume-shear coupling, correlated slips occur at 45° with respect to the principal axis of the stress tensor, as this is the orientation in which the maximum shear stress occurs. However, in the presence of volume-shear coupling, this angle changes. We will address this effect now.

The one-site modeling of the previous section is the base for a spatially extended model in which each site is characterized by its strain and its volume degree of freedom. Details of the model have been presented elsewhere[16–18], and here we only state its more relevant characteristics. We work with three functions $e_1(\mathbf{r})$, $e_2(\mathbf{r})$, $e_3(\mathbf{r})$, that represent one volume and two shear degrees of freedom at each position. Volume-shear coupling is obtained by the use of a potential energy qualitatively similar to that in Eq. (8), but also with some differences due in part to technical reasons. First of all, taking into account that physically e_2 and e_3 differ only by a spatial rotation of 45° , we should consider $(e_2^2 + e_3^2)$ as the vari-

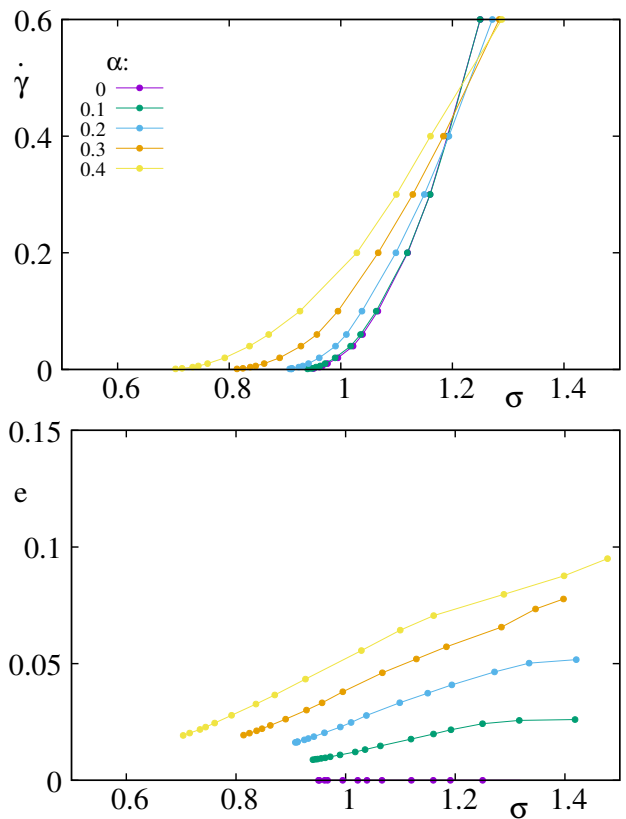


FIG. 3: (a) Flow-curves ($\dot{\gamma}$ vs σ) at different values of the volume-shear coupling parameter α , as indicated. (b) The corresponding curves for the average volume change (with respect to the equilibrium(?) $e_1 = 0$ value). The qualitative behavior of the model is consistent with the results obtained in the one-particle model (Fig. 2).

able to couple to e_1 through a parameter α similar to that used in the previous section. However notice that in our implementation using finite differences onto a square lattice, the variables e_1 and e_2 are calculated on the nodes of this lattice, whereas e_3 is defined at the centers of the plaquettes. This makes a possible coupling between e_1 and e_3 a non-local one in the present numerical scheme, producing spurious effects that require special care to be avoided. This is certainly a point that will deserve further attention. However, since the external driving is applied on the e_2 direction we may also expect that the main effect we are interested in can be captured by coupling e_1 to e_2 only, leaving e_3 evolve without any coupling to e_1 . Therefore we will model the local potential energy as

$$V(e_1, e_2, e_3) = \frac{B}{2}e_1^2 + [1 + \tanh(\alpha e_1)]U_2(e_2) + U_3(e_3) \quad (11)$$

The functions U_2 , U_3 will be taken to be of the “smooth” type, but with a stochastic ingredient, this stochasticity being totally uncorrelated in different spatial positions. We proceed as follows. We define a value e_0 (either e_{20} or e_{30} for e_2 or e_3) and define the corresponding U to be

given by

$$U = \sin\left(\frac{(e - e_0)\pi}{\Delta}\right) \quad (12)$$

where Δ is a random variable taken from a uniform distribution between 0.5 and 1. We monitor along the simulation the values of $e - e_0$ and compare against the value of Δ . Each time we detect $\pm(e - e_0) > \Delta$ a new value Δ_{new} is defined, and e_0 is redefined to $e_0 \pm (\Delta + \Delta_{new})$. In this form we implement an independent stochastic disordered potentials for e_2 and e_3 at every position in the sample. The equations of motion of the model are therefore of the form

$$\dot{e}_i = -\frac{dV}{de_i} \quad (13)$$

that however must be solved taking into account that there is a constrain among e_1 , e_2 , and e_3 that must be fulfilled (the so called St Venant constrain [20]), and that is imposed by the appropriate use of Lagrange multipliers [16–18].

We present some flow and volume curves for this model in Fig. 3. We observe in the extended system the same qualitative features obtained for the one particle case (Fig. 2), namely a shift of curves to the left and an increase in system volume as α is increased. A more detailed inspection of the spatial distribution of deformation reveals a particular effect associated to a non-zero value of α . In Fig. 4 we see plots of accumulated strain e_2 in the system, at a relatively large value of $\dot{\gamma} = 0.1$, in systems with different values of α . In Fig. 4 the angle of correlation of plastic activity is clearly visible, and is observed that this angle deviates from 45° when $\alpha \neq 0$. By calculating a correlation function on spatial configurations as those in Fig. 4, the angle of maximum correlation can be determined with good precision. The result as a function of α is seen in Fig. 5. The angle is 45° in the case $\alpha = 0$, but deviates from this value when $\alpha \neq 0$, the deviation being linear with α .

The orientation correlation of plastic activity (and ultimately of directions of shear bands) with respect to principal stress directions is an important feature in many practical situations, so the reason for this reorientation is worth to be explored in more detail. When $\alpha = 0$ the failure planes are determined by the condition of maximum shear stress, and this always occur at 45° with respect to the principal axis (in the present simulations they being the x and y axis). However, if $\alpha \neq 0$ the stress normal to the failure plane plays a role as a reduction in normal stress favors slip by reducing the critical stress. Therefore there is rotation of the slip planes with a normal that tends to align with the axis in which the compressive stress is minimum. The amount of this rotation depends on how much the critical shear stress depends on the perpendicular stress. We now analyze the problem quantitatively.

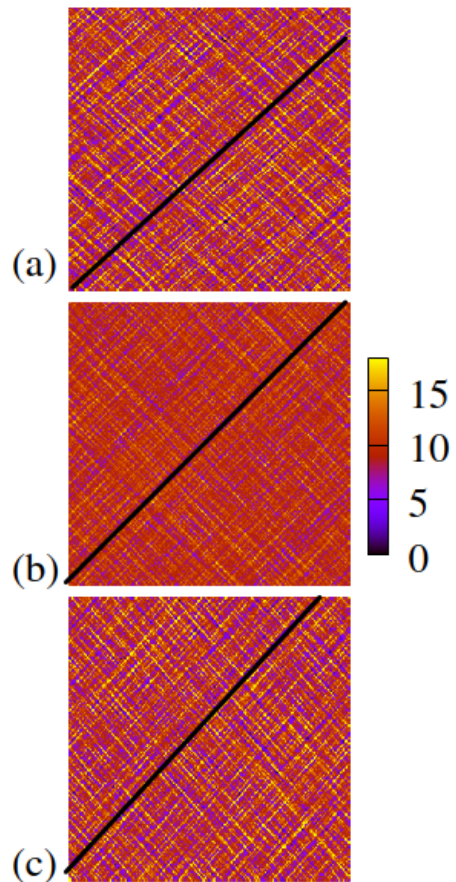


FIG. 4: Snapshots of accumulated deformation in the system at different values of the volume-shear coupling parameter: $\alpha = 0.2$ (a), 0 (b), and -0.2 (c). Note the change in the correlation between slips in different positions of the sample (highlighted by the diagonal or off-diagonal straight black lines).

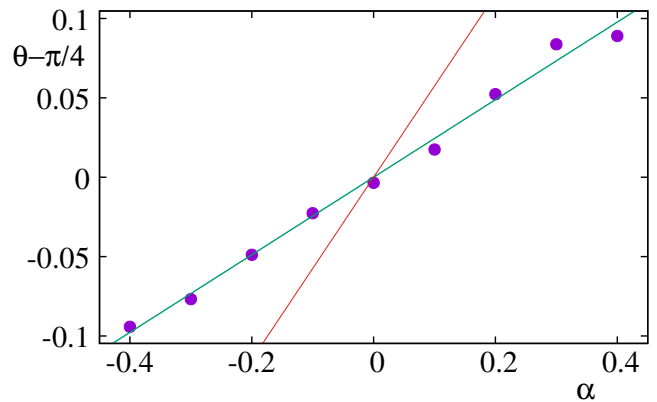


FIG. 5: Angle of maximum correlation between slips in the sample as a function of α . Dots are the measured values, and green straight line is the linear fit $\theta = \pi/4 + 0.21\alpha$. The red line is the result contained in Eq. (25).

A. Mohr-Coulomb theory

Consider a sample that is subject to (compressive) x and y stresses σ_x and σ_y , and suppose we want to analyze the possibility of a slip along a plane that forms an angle θ with respect to the x axis. Along this plane, the shear (τ) and normal (σ_n) stresses are given by

$$\sigma_n(\theta) = \frac{\sigma_x + \sigma_y}{2} + \cos(2\theta) \frac{\sigma_x - \sigma_y}{2} \quad (14)$$

$$\tau(\theta) = \sin(2\theta) \frac{\sigma_x - \sigma_y}{2} \quad (15)$$

In the classical Mohr-Coulomb approach[2], the failure criterion corresponds to a static friction condition: the stress τ must be larger than the normal stress multiplied by some friction coefficient μ . This normal stress includes in general a cohesive part σ_0 in addition to the external contribution σ_n . In the end, the failure condition at a given angle θ is

$$\tau(\theta) > (\sigma_0 + \sigma_n(\theta))\mu \quad (16)$$

Combining (15) and (16) we obtain that yielding at an angle θ may occur if

$$(\sin(2\theta) - \mu \cos(2\theta))(\sigma_x - \sigma_y) > (2\sigma_0 + \sigma_x + \sigma_y)\mu \quad (17)$$

The weakest direction in the sample is the angle θ_0 at which the angular function in this expression is maximum. This is easily determined as (we assume $\sigma_x > \sigma_y$)

$$\theta_0 = \frac{1}{2} \text{atan}(-\mu^{-1}) \quad (18)$$

This is the required expression. It gives the angle at which yielding will first occur, and therefore the angle of correlated plastic deformations in the sample. As in most cases the deviation of θ_0 with respect to $\pi/4$ is small, we can approximate Eq (18) as

$$\theta_0 \simeq \pm \left(\frac{\pi}{4} + \frac{\mu}{2} \right) \quad (19)$$

Yet, for this expressions to be useful, we need to know the value of μ for our sample. Clearly, μ depends on the volume-shear coupling parameter α . If $\alpha = 0$ there will not be any effect of the normal stress on the critical shear stress, and $\mu = 0$, for which the classical $\theta_0 = \pi/4$ is obtained. In order to get the value of μ for a general α , we proceed as follows. Reinserting expression (18) into (17) we obtain at criticality

$$\sigma_x - \sigma_y = \frac{\mu(2\sigma_0 + \sigma_x + \sigma_y)}{\sqrt{1 + \mu^2}} \quad (20)$$

Although in Section II we have considered only cases in which $\sigma_x + \sigma_y = 0$, here we will take advantage of the

possibility that this quantity is non-zero, defining a compressive stress $\sigma_{comp} \equiv (\sigma_x + \sigma_y)/2$. Also we will call $\sigma_c \equiv (\sigma_x - \sigma_y)/2$, as this is what we have used in Section II as the critical shear stress in the system. Considering that when α is small, so is μ , we linearize expression (20) and obtain

$$\sigma_c = \mu(\alpha)(\sigma_0(\alpha) + \sigma_{comp}) \quad (21)$$

where the dependence of μ and σ_0 on α have been explicitly indicated. We can determine the dependence of μ on α by measuring how the critical shear stress in the sample depends on the application of a uniform compressive stress σ_{comp} . We see that with respect of this compressive stress, the critical shear stress behaves as

$$\Delta\sigma_c \equiv (\sigma_c - \mu\sigma_0) = \mu(\alpha)\sigma_{comp} \quad (22)$$

A compressive stress can be easily added in our numerical model, and the variation of σ_c calculated as a function of σ_{comp} and α . The results (shown in Fig. 6) are very well fitted by an expression of the form

$$\Delta\sigma_c = 1.1\alpha\sigma_{comp} \quad (23)$$

that compared with the previous expression (22) gives the dependence

$$\mu(\alpha) \simeq 1.1\alpha \quad (24)$$

This expression can now be used in Eq. (19) to obtain

$$\theta_0 \simeq \pm \left(\frac{\pi}{4} + 0.55\alpha \right) \quad (25)$$

which is the Mohr-Coulomb prediction for the angle of plastic slips in terms of the volume-shear coupling parameter α . This linear function is plotted on top of the numerical results in Fig. 5. The linear dependence of θ_0 on α reproduces the trend of the numerical results, however the present analysis predicts a slope that is about a factor between two and three larger than the one observed. At the moment, we do not have a reasonable explanation for this discrepancy.

IV. NON-UNIFORM YIELDING CAUSED BY VOLUME-SHEAR COUPLING

An important phenomenon that may occur in the flowing of amorphous materials is localization of the deformation. In some cases (as it occurs in metallic glasses, see next section) this localization is a non-equilibrium phenomenon typically associated to the preparation of the sample. In other cases, this localization occurs at equilibrium and this is the situation that is addressed here. In Ref. [21] a stability analysis was performed for a flowing system that has, apart from the normal shear variables, additional scalar degrees of freedom taken to

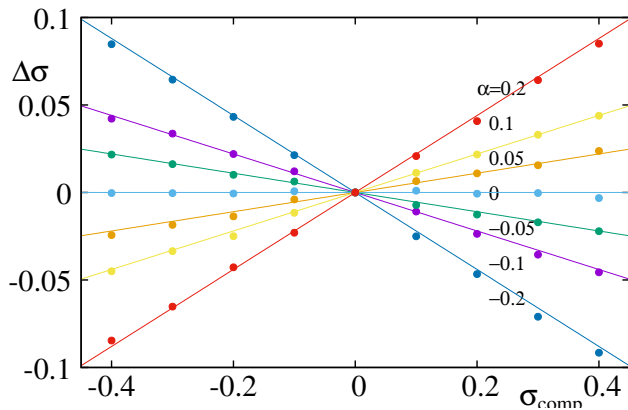


FIG. 6: Variation of the critical force $\Delta\sigma_c$ as a function of the compressive stress σ_{comp} (with reference to its value at zero compressive stress). Dots are the results of the simulations, for different values of α . Lines are plots of the function $1.1\alpha\sigma_{comp}$, which provides a very good fitting of the numerical results.

represent the concentration of solute molecules in the material. The analysis made is quite general, and essentially applies also to our case in which the additional scalar variables can be considered to be the value of the local density in the system. Restricted to a two-dimensional situation appropriate to our case, the result of the analysis indicates that there are two different kinds of instabilities. In one of them, instability is purely mechanical, with the density degree of freedom playing no important role. The signature of such an instability is a flow curve that has a reentrance, namely a region in which stress diminishes as strain rate increases. This kind of instability is analogous to that producing phase separation in a one component fluid, such as in the liquid-gas transition. In physical terms, this instability occurs in the following way. If a layers of the system that is shearing at some value of strain rate suffers a perturbation that increases it, then it would require less stress to maintain the new strain rate. But as the applied stress is kept fixed, this will produce an additional increase of strain rate, leading to an instability. This situation is known to occur for instance in cases in which there are aging mechanisms in the system[16, 22–27]. It may thus happen that non-flowing regions keep a well aged state that is more rigid, and therefore do not flow, while flowing regions, being unable to age sufficiently, have a lower critical stress and are maintained in a flowing state. Recently[28], another possibility has been suggested leading to the same phenomenology, namely the case in which the bulk modulus of the materials is very small. In that case the origin of the instability can be traced back to the effective softening of the material when strain rate is reduced, leading to a more strongly pinned state and to a reentrance of the flow curve that is responsible of the mechanical instability.

In addition to this kind of mechanical instability, it

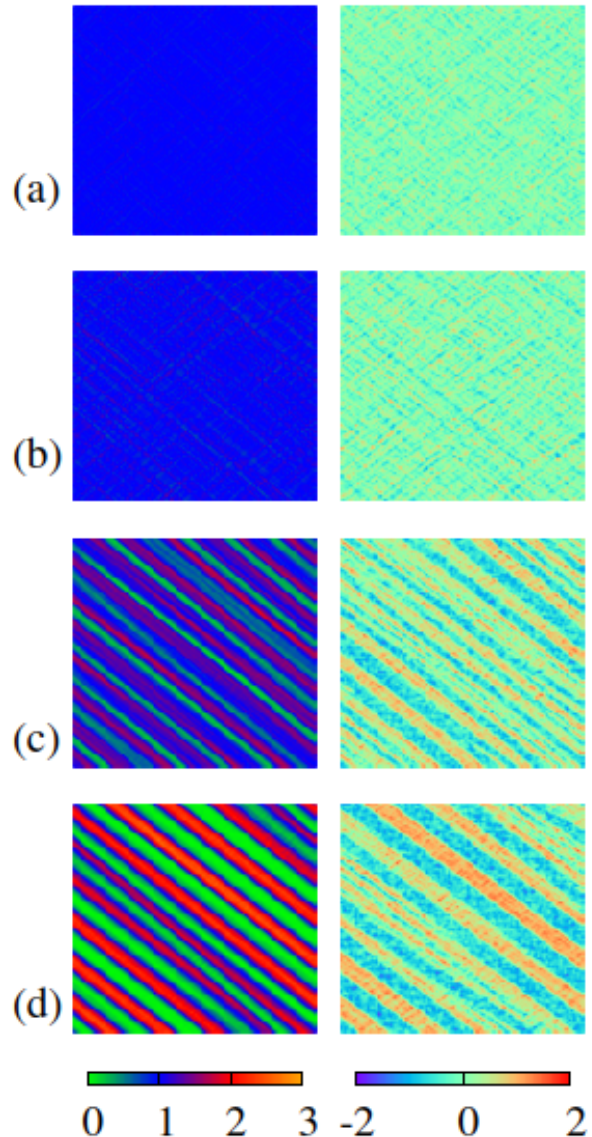


FIG. 7: Accumulated strain deformation (left column, the scale value 1 corresponds to the nominal average deformation in all cases) and instantaneous values of e_1 (right column) in simulations at the same value of $\dot{\gamma} = 0.1$, in systems with different values of shear-volume coupling parameter α , namely $\alpha = 0.1$ (a), 0.2 (b), 0.3 (c), and 0.4 (d) (system size is 128×128). The long term deformation is uniform in the first two cases, but is inhomogeneous in the last two.

was found [21] that the coupling to the concentration degree of freedom can produce a breaking of the uniform flow, even in the absence of any strong feature of the flow curve. This instability is qualitatively understood in the following way.[10, 29, 30] If on an originally uniform yielding state, a fluctuation in some part of the sample produces an increase in strain rate, then that part of the system will also experience an expansion which in turn produces a decrease in the effective viscosity and a further

increase in the strain rate. This process can eventually lead to an instability which however does not manifest clearly in the form of the flow curve of the system.

We have observed this kind of instability in the present model, in the case in which α is large enough. The numerical evidence is contained in Fig. 7. There in the left column we observe plots of the accumulated deformation in the system in a rather long time window at a constant value of $\dot{\gamma} = 0.1$, and for different values of α . For low α ($\alpha \lesssim 0.2$) the deformation is uniform, whereas for larger α we clearly see that there are regions in the system that have not yielded at all, showing the non-uniform yielding in this case. The instantaneous values of the volume variable e_1 across the system (right column in Fig. 7) show also a clear correlation with the deformation in the large α cases, with the sample flowing in regions in which the local volume is well above the average value. Stuck regions instead correspond to compressed sample regions, with values of e_1 below the average.

V. VOLUME-SHEAR COUPLING IN ANNEALED SAMPLES. THE CASE OF METALLIC GLASSES

The effects of volume-shear coupling that have been discussed so far all correspond to situations of dynamical equilibrium in the system, or in other words, they all describe stationary situations. There are other situation however, in which we are interested in transient (although probably long-lived) properties of the system. In many cases this occurs when we do an experiment on a sample prepared by some ad-hoc protocol, that leaves it in an out of equilibrium configuration. In concrete we want to refer to the case of metallic glasses.[12–15] They are usually prepared by annealing from a melt, and its configuration cannot by any means be considered as an equilibrium one. When the metallic glass is submitted to an external load, the appearance of a shear band is a highly non-equilibrium process. Yet the kind of models we have presented can be used to model this scenario, and in particular the effect of volume fluctuations on the behavior of this kind of materials.

The key to mimic the behavior of a metallic glass under shear is to start with an initial configuration that appropriately incorporates the annealed nature of the experimental initial state. In our model we can produce a starting configuration that is more stable than the stationary one after long deformation by adjusting the local disorder potentials at different sites[16]. The local potentials are characterized by the values of e_{20} and e_{30} , defining the local equilibrium strain, and the corresponding values of Δ measuring the extent of the corresponding basin. In a stationary situations as those considered so far, the values of e_0 have some dynamically generated dispersion, and Δ is randomly chose from a uniform distribution between 0.5 and 1.0. We can construct a more stable starting sample by appropriately modifying e_0 and/or Δ .

The possibility that we will implement here is to anneal the sample (before strain is applied) by allowing the values of e_{20} and e_{30} to relax towards more stable configurations. This is the scheme that was originally used in Ref. [16]. Here we apply the same protocol in the presence of volume-shear coupling. In concrete, we first generate a stationary state by running a long simulation with a small value of $\dot{\gamma} = 0.001$. In this situation we stop driving (setting $\dot{\gamma} = 0$) and perform an annealing process that consists in adapting dynamically the values of e_{20} and e_{30} according to

$$\dot{e}_{20} \sim \nabla^2 e_{20} \quad (26)$$

$$\dot{e}_{30} \sim \nabla^2 e_{30} \quad (27)$$

while at the same time continuing to relax the values of e_1 , e_2 , and e_3 following the standard evolution equations of the model. This produces, after annealing for some period of time, a configuration that is more relaxed than the stationary state, because now the values of e_{20} and e_{30} are strongly correlated spatially, and the surface is effectively more pinned. Finally, we stop the relaxation of e_{20} and e_{30} , generating the starting configuration. We present results in the extreme case in which relaxation is performed during a very long time, and therefore, the values of e_{20} and e_{30} acquire a uniform value across the system. From this initial configuration strain is increases at a low strain rate $\dot{\gamma} = 0.001$, and the stress is numerically evaluated.

The results obtained are shown in Fig. 8 for systems with different intensity of volume-shear coupling. All curves in Fig. 8 display a stress overshoot that is the hallmark of annealed samples that are more stable than the asymptotic dynamic equilibrium state. Yet we see that the amplitude of the stress overshoot is much more pronounced in samples with larger value of α . In order to have a deeper understanding of the effect of α we must investigate the local distribution of deformation in the samples. In Fig. 8 we have indicated three strain windows, labelled (A), (B), and (C). The local distribution of accumulated strain in each of these windows is indicated in Fig. 9 for three different values of α , namely $\alpha = 0, 0.2, 0.4$.

The case $\alpha = 0$ serves as a reference, and is similar to that studied in Ref. [16]. We emphasize that even in this case, an overshoot is observed in the stress-strain curve (Fig. 8). In the strain window (A), when stress is still increasing in the system, we observe rather isolated plastic events that do not yet organize across the sample. In strain windows (B) and (C) instead, when the stress peak has been overpassed, the plastic strain is localized in a spatial region that can be termed a shear band. The reason for this behavior is that in the shear band the system was forced to escape from the initial annealed state, and its critical stress is now lower than in the still annealed part, that is non flowing. This stabilized the shear band in the system. This shear band widens when strain is increased as $\sim \gamma^{1/2}$ [31–33]. Notice that the strain local-

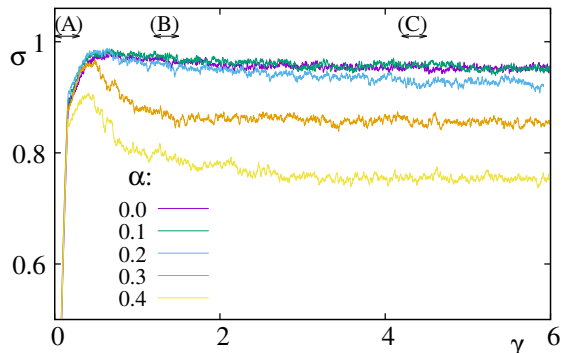


FIG. 8: Stress-strain curves (using $\dot{\gamma} = 0.001$) in samples with different values of α as indicated, after an annealing in the initial state, as described in the text. All curves display a stress overshoot above the asymptotic values, but the effect is much stronger in samples with large α .

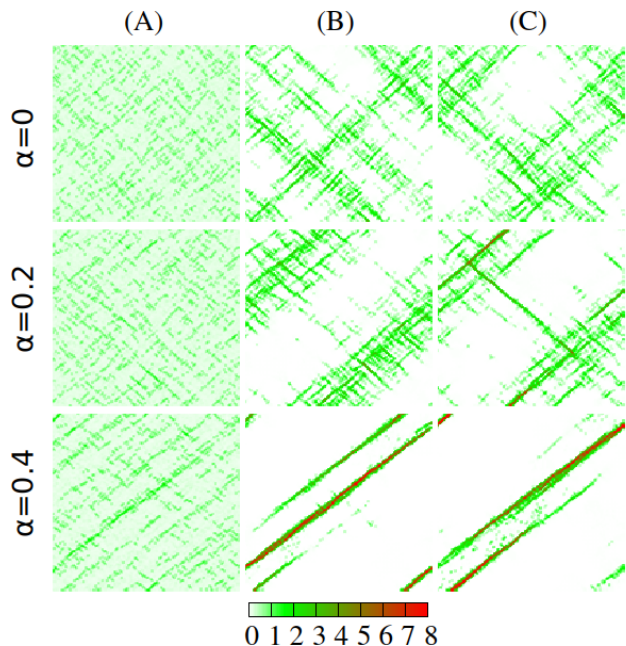


FIG. 9: Accumulated spatial distribution of strain in the three strain windows indicated in Fig. 8, for three different values of α . Although for all values of α we observe strain localization, the effect for larger α produces a much narrow shear band.

ization at $\alpha = 0$ is not observable in the distribution of the volume variable e_1 (Fig. 10(a)).

The case of a finite shear-volume coupling ($\alpha > 0$) produces some quantitative differences and also some qualitative new phenomena. First of all, in Fig. 8 we clearly see how the increasing part of the stress-strain curve is not much dependent on the value of α , and in fact, the spatial distribution of the deformation in strain window (A) shows a rather uniform deformation distribution independently of α . However, after the stress peak is overcome, the stress decrease is much larger in samples with

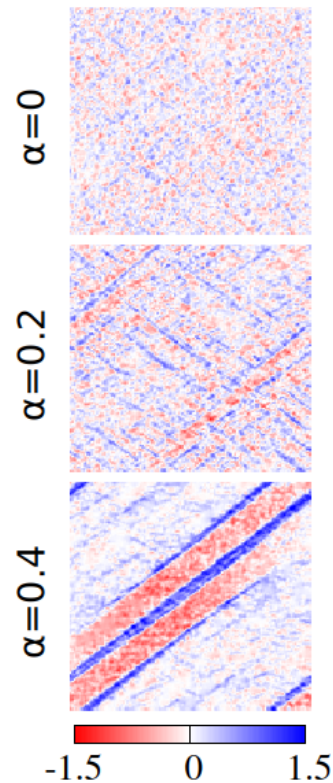


FIG. 10: Instantaneous distribution of the volumetric e_1 variable, right after the time window (C), for the three different values of α presented in Fig. 9. The position of the shear band in the system can be inferred from the distribution of e_1 in the case in which α is large.

large α . The analysis of the spatial distribution of deformation reveals that the accumulated strain at finite α shows a stronger tendency to become more localized. Most remarkably, for values of α where we had previously observed an instability of the homogeneous deformation situation ($\alpha \gtrsim 0.2$, see Fig. 7), we now observe that only a very thin shear band is activated in the system, with all the rest remaining in a rigid configuration. This is very clear in the plots corresponding to $\alpha = 0.4$ in Fig. 9. Notice that as the shear band does not run exactly along the diagonal (see Section III), and because of the periodic boundary conditions, there are some "mirror images" of the shear band, giving the impression of a few different shear bands in the system.

We think the most remarkable effect of a finite α manifests in the spatial distribution of the e_1 variable (Fig. 10). While for $\alpha = 0$ we did not have any clue of the strain localization from the distribution of e_1 , in the finite α case, particularly when $\alpha \gtrsim 0.2$ this is not so. In fact, in Fig. 10(c) we clearly observe that the localization of the shear band corresponds to a region where the system is expanded (therefore facilitating the shearing of the system in this region). We emphasize that if we stop

increasing the strain in the system, or even if strain is reduced as necessary to reach a state of zero stress, the spatial distribution of e_1 remains essentially at the configuration shown in Fig. 10. Therefore, the localization of the shear band where the system has yielded can be evaluated after the full process took place, by localizing the regions of the sample that are expanded with respect to the starting configuration.

VI. SUMMARY AND CONCLUSIONS

In this work, we have introduced a mesoscopic model for the yielding behavior of amorphous materials incorporating the possibility of volume-shear coupling. This ingredient is acknowledged to have important experimental consequences, but it has not been previously considered in numerical models of the yielding transition. Volume-shear coupling produces a number of effect in the phenomenology of shear stress materials. It generates a change in the direction of the shear bands in the system. Our numerical simulations clearly show this angular deviation. We have applied the classical Mohr-Coulomb theory to predict the deviation, and find results that qualitatively agree with the simulations but that misses the quantitative effect by a factor between two and three. We do not have a clear explanation for this discrepancy. Also, we have observed that when the volume-shear coupling is strong enough, there is a tendency in the system to produce a non-uniform deformation. There are regions that become more expanded, and therefore yield more

easily, while others remain in a more compact configuration, and do not yield at all. Finally, we have briefly discussed the effect of volume-shear coupling in cases in which the sample is initially annealed to obtain a starting configuration that is more stable than the asymptotic configuration that appears as a stationary state after a very long deformation time. This situation is particularly adapted to the phenomenology of metallic glasses. Now, when the sample is strained, the stress in the system develops a peak before smoothly decaying to the asymptotic stress value. The case of no volume shear-coupling has been studied in previous works [16, 32, 34] and it was observed that after the strain corresponding to the stress maximum is exceeded, the deformation in the sample localizes in a shear band. This band progressively widens with further deformation as discussed in Ref. [31, 33]. Now in the case in which there is volume-shear coupling, particularly when this is large, we observe that the shear band that appears in the system is very thin, and we do not detect clearly that it widens as deformation proceeds. We observed that in the region of this thin band the system is expanded, and this expansion remains even if deformation is stopped and stress relaxes back to zero. All these findings point to the utility of the present kind of model in the study of shear stress materials for which shear-volume coupling is important.

VII. ACKNOWLEDGMENTS

I thank Ezequiel Ferrero for helpful stimulating discussions.

-
- [1] Reynolds, O. (1885). *Philosophical Magazine*. Series 5. 20 (127): 469–481.
 - [2] R.M.Nedderman. *Statics and Kinematics of Granular Materials*. Cambridge University Press, 1992.
 - [3] Culling, W. E. H., *J. Geol.* 71, 127–161 (1963).
 - [4] Dietrich, W. E. et al. *Geophys. Monogr. Am. Geophys. Union* 135, 103–132 (2003).
 - [5] Roering, J. J., Kirchner, J. W., and Dietrich, W. E., *J. Geophys. Res. Solid Earth* 106, 16499–16513 (2001).
 - [6] D. J. Jerolmack and K. E. Daniels *Nat. Rev. Phys.* 1, 716–730 (2019).
 - [7] D. Bonn, M. M. Denn, L. Berthier, T. Divoux, and S. Manneville, *Rev. Mod. Phys.* 89, 035005 (2017).
 - [8] A. Nicolas, E. E. Ferrero, K. Martens, and J.-L. Barrat, *Rev. Mod. Phys.* 90, 045006 (2018)
 - [9] G. Ovarlez, S. Cohen-Addad, K. Krishan, J. Goyon, and P. Coussot *J. Non-Newton Fluid Mech.* 193 (2013) 68–79.
 - [10] Besseling, R., L. I. P. Ballesta, G. Petekidis, M. Cates, and W. Poon (2010), *Phys. Rev. Lett.* 105, 268301.
 - [11] P. Coussot, *J. Non-Newton Fluid Mech.* 211 (2014) 31–49.
 - [12] C. Tang, H. Peng, Y. Chen, and M. Ferry, *Journal of Applied Physics* 120, 235101 (2016)
 - [13] A.L.Greer, Y.Q.Cheng, and E.Ma *Mat. Sci. Eng. R*, 74, 71–132, (2013).
 - [14] S. Ogata, F. Shimizu, J. Li, M. Wakeda, and Y. Shibutani *Intermetallics* 14 (2006) 1033–1037
 - [15] C. Zhong, H. Zhang, Q. P. Cao, X. D. Wang, D. X. Zhang, U. Ramamurty, and J. Z. Jiang *Sci. Rep.* 6, 30935 (2016).
 - [16] Jagla, E. A. (2007), *Phys. Rev. E* 76, 046119.
 - [17] I. Fernández Aguirre and E. A. Jagla *Phys. Rev. E* 98, 013002 (2018).
 - [18] E.E. Ferrero, E.A. Jagla *Soft matter* 15 (44), 9041-9055 (2018).
 - [19] V. L. Popov and J. A. T. Gray, *ZAMM. Z. Angew. Math. Mech.* 92, 683 (2012).
 - [20] D. Chandrasekharaiah and L. Debnath, *Continuum Mechanics* (Academic Press, San Diego, 1994).
 - [21] V. Schmitt, C. M. Marques, and F. Lequeux *Phys. Rev. E* 52, 4009 (1995).
 - [22] Picard, G., A. Ajdari, L. Bocquet, and F. Lequeux, *Phys. Rev. E* 66, 051501 (2002).
 - [23] Olmsted, P. D., *Rheol. Acta* 47, 283 (2008).
 - [24] Divoux, T., M. A. Fardin, S. Manneville, and S. Lerouge, *Annu. Rev. Fluid Mech.* 48, 81103 (2016).
 - [25] Coussot, P., Q. D. Nguyen, H. T. Huynh, and D. Bonn, *Phys. Rev. Lett.* 88, 175501 (2002).
 - [26] Mujumdar, A., A. N. Beris, and B. Metzner, *J. Non-Newtonian Fluid Mech.* 102, 157 (2002).

- [27] Martens, K., L. Bocquet, and J.-L. Barrat, *Soft Matter* 8, 4197 (2012)
- [28] E.A. Jagla, *J. Stat. Mech.* ... (2022).
- [29] Fall, A., F. Bertrand, G. Ovarlez, and D. Bonn, *Phys. Rev. Lett.* 103, 178301 (2009).
- [30] Ovarlez, G., F. Bertrand, and S. Rodts, *J. Rheol.* 50, 259 (2006).
- [31] Jagla E. A., *J. Stat. Mech.* P12025 (2010).
- [32] Y. Shi, M. B. Katz, H. Li, and M. L. Falk, *Phys. Rev. Lett.* 98, 185505 (2007).
- [33] D. D. Alix-Williams and M. L. Falk, *Phys. Rev. E* 98, 053002 (2018).
- [34] Vandembroucq, D., and S. Roux (2011), *Phys. Rev. B* 84, 134210.